Fabrication of Isolated Metal–Organic Polyhedra in Confined Cavities: Adsorbents/Catalysts with Unusual Dispersity and Activity

Ying-Hu Kang,[†] Xiao-Dan Liu,[†] Ni Yan,[†] Yao Jiang,[†] Xiao-Qin Liu,[†] Lin-Bing Sun,*,[†] and Jian-Rong Li*,[‡]

[†]State Key Laboratory of Materials-Oriented Chemical Engineering, Jiangsu National Synergetic Innovation Center for Advanced Materials (SICAM), College of Chemistry and Chemical Engineering, Nanjing Tech University, Nanjing 210009, China

[‡]Beijing Key Laboratory for Green Catalysis and Separation, College of Environmental and Energy Engineering, Beijing University of Technology, Beijing 100124, China

Ⓢ *Supporting Information*

ABSTRACT: Metal–organic polyhedra (MOPs) have attracted great attention due to their intriguing structure. However, the applications of MOPs are severely hindered by two shortcomings, namely low dispersity and poor stability. Here we report the introduction of four MOPs (constructed from dicopper and carboxylates) to cavity-structured mesoporous silica SBA-16 via a double-solvent strategy to overcome both shortcomings simultaneously. By judicious design, the dimension of MOPs is just between the size of cavities and entrances of SBA-16, MOP molecules are thus confined in the cavities. This leads to the formation of isolated MOPs with unusual dispersion, making the active sites highly accessible. Hence, the adsorption capacity on carbon dioxide and propene as well as catalytic performance on ring opening are much superior to bulk MOPs. More importantly, the structure and catalytic activity of MOPs in confined cavities are well preserved after exposure to humid atmosphere, whereas those of bulk MOPs are degraded seriously.

Metal–organic polyhedra (MOPs, also known as molecular polyhedra, nanoballs, and nanocages) are discrete molecular architectures fabricated through the coordination of metal ions and organic ligands.[1] Due to their fascinating structure, relevance to biological self-assembled systems, and various potential applications (e.g., adsorption, catalysis, and molecule inclusion), MOPs have attracted significant attention in recent years.[2] However, the applications of MOPs are severely hindered by two factors, namely easy aggregation of MOP molecules and poor stability. For the first factor, aggregation is almost inevitable after activation (i.e., the removal of guest molecules to form accessible active sites), which is compulsory for both MOPs and metal–organic frameworks (MOFs) before utilization.[3] Owing to the interconnected channels in MOFs, the accessibility of active sites is greatly improved after activation. Nevertheless, serious aggregation of MOP molecules occurs after activation, leading to the blockage of active sites by each other.[4] This compromises the performance of MOPs seriously, and in some cases MOPs even do not show any detectable adsorptive and catalytic activity at all. For the second factor, MOPs are constructed by metal–organic coordination bonds, giving rise to weak hydrostability. Because the coordination bonds are easily attacked by even a trace of water, some MOPs are even unstable at atmospheric moisture levels. Despite great challenges, the development of an efficient method to enhance the dispersity and stability of MOPs is extremely desirable.

Another group of porous materials that have received great interest are mesoporous silicas, which possess large pore volumes, ordered pore structure, and tunable symmetries (e.g., hexagonal, cubic, and lamellar).[5] The pore sizes on a nanoscale (adjustable from 2 to 50 nm) make mesoporous silicas valuable as supports to disperse a range of guests including nanoparticles, enzymes, and drug macromolecules.[6] Taking into consideration that MOPs have molecular dimensions of several nanometers, mesoporous silicas should be an ideal accommodation for MOP molecules. Among mesoporous silicas, 3D cubic structured cavity-like materials, which have large cavities interconnected by small pore entrances, are of great interest.[7] The large cavities should be able to accommodate MOP molecules, whereas the small pore entrances prevent them from leaching. MOPs are thus expected to confine in nanoscale cavities, forming isolated molecules with high dispersity. As a result, aggregation that happens for bulk MOPs may be avoided completely, and the active sites become accessible. Furthermore, due to the special microenvironment in nanoscale cavities, the confinement of MOPs is expected to enhance the stability. To our knowledge, however, reports concerning the confinement of MOPs in nanoscale cavities are very scarce, if any.

Here we report for the first time the confinement of MOP molecules in the cavities of mesoporous silica by using a double-solvent (DS) strategy (Figure 1). Four MOPs with an identical geometry but different ligand functionality were carefully selected (Figure S1). Taking into account that the dimension of these MOPs is ~3 nm, a typical cavity-structured mesoporous silica, SBA-16, with a cavity size of ~6 nm and a pore entrance of ~2 nm was employed to confine MOP molecules. By use of the DS strategy, the high interfacial tension between hydrophobic solvent and hydrophilic solution (containing precursors) can drive the precursors into hydrophilic cavities. This leads to the construction of highly dispersed and amount-controllable MOPs in the cavities of SBA-16, while limits the formation of MOPs outside the pores. Our results show that the selective growth of MOPs in the cavities is successfully achieved, since the dimension of MOPs is just between the size of cavities and
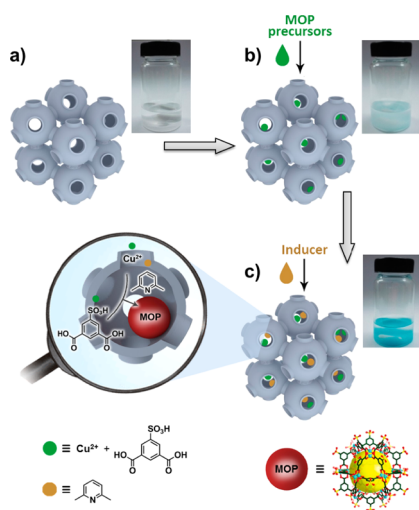
Figure 1. Schematic diagram and photographs for the fabrication of MOP-SO$_3$H in the cavities of mesoporous silica SBA-16 using the DS strategy. (a) Dispersion of SBA-16 in hydrophobic *n*-hexane; (b) addition of the hydrophilic methanol solution containing MOP precursors (metal ions and ligands); (c) addition of the inducer (base) for MOPs formation.

Figure 2. (a) PXRD patterns and (b) UV−vis spectra of the samples SBA-16, MS-SO$_3$H, M′S-SO$_3$H, and MOP-SO$_3$H. (c) TEM and (d) STEM images and elemental mapping of the composite MS-SO$_3$H.

pore entrances. Isolated MOP molecules are thus formed, making the active sites in MOPs highly accessible to adsorbates and reactants. We demonstrate that, in contrast to aggregated bulk MOPs, the isolated MOPs exhibit much superior adsorption capacity and catalytic performance. Furthermore, the stability of MOPs subjected to confinement in cavities is greatly improved. After exposure in humid atmosphere, the confined MOPs well preserve their structure and catalytic activity, which is quite different from bulk MOPs whose structure and catalytic activity are seriously weakened.

The first MOP employed is MOP-SO$_3$H, which is synthesized from Cu(NO$_3$)$_2$ and 5-sulfonic-1,3-benzenedicarboxylic acid (H$_2$L1).[8] Structurally, MOP-SO$_3$H has a cuboctahedral geometry when the 12 dicopper units are viewed as vertices and the ligands are viewed as edges. The DS strategy for the introduction of MOPs to mesoporous silica SBA-16 is illustrated in Figure 1. SBA-16 was added to hydrophobic *n*-hexane, followed by successive addition of a small amount of hydrophilic methanol solution containing precursors ($V_{solution} < V_{pore\ of\ SBA-16}$) and the inducer 2,6-lutidine. Because the inner surface of SBA-16 is more hydrophilic than the outer surface, the small amount of hydrophilic methanol solution easily enters the pores by capillary force. Self-assembly of MOPs thus takes place in SBA-16 pores in the presence of 2,6-lutidine. By changing the amount of precursors, the MOPs@SBA-16 composites containing one or two MOP(s) in one cavity can be obtained and denoted as MS-SO$_3$H and M′S-SO$_3$H, respectively.

The mesoporous structure of samples was first characterized. In low-angle powder X-ray diffraction (PXRD) patterns, MOPs-containing composites show similar diffraction peaks to pristine SBA-16 (Figure 2a), which corresponds to the cubic pore regularity of the *Im3m* space group. TEM images of MOPs@SBA-16 composites at different levels of magnification present periodic ordering of mesostructure (Figures 2c and S2), which is comparable to pristine SBA-16 (Figure S3). These images thus confirm the low-angle PXRD results, pointing out that the long-range pore ordering of SBA-16 is well preserved after the introduction of MOPs.
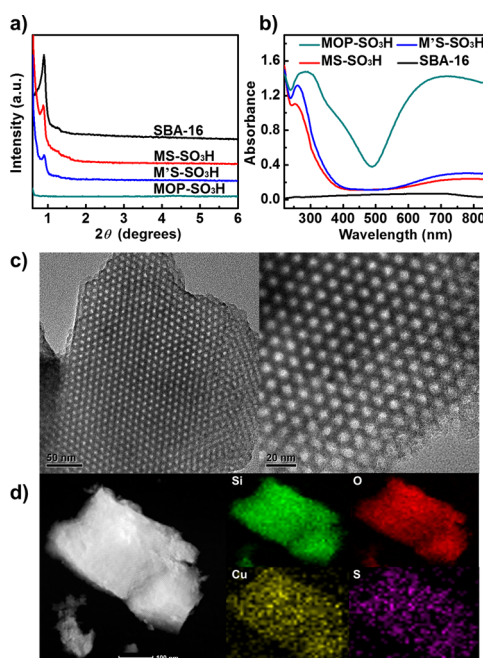
The UV−vis spectrum of MOP-SO$_3$H exhibits an intense adsorption peak at around 695 nm (Figure 2b), which is characteristic of the dicopper paddlewheel units.[8,9] Because the tetrahedral coordinated SiO$_4$ units have no adsorption in the UV−vis range, pristine mesoporous silica SBA-16 does not have any adsorption peaks. In the case of MOPs@SBA-16 composites, there is an adsorption peak at 695 nm originated from MOPs despite the intensity is lower in comparison with pure MOPs. This suggests that MOPs are successfully introduced to mesoporous silica and that the dicopper paddlewheel units remain intact in the composites. To gain insights into the distribution of MOPs in mesoporous silica, elemental mappings were taken (Figures 2d and S2). In addition to Si and O derived from SBA-16, the elements Cu and S stemmed from MOPs are detected. More importantly, these elements are homogeneously distributed in the whole sample. In wide-angle PXRD patterns, pristine SBA-16 gives a broad diffraction peak at about 23° ascribed to amorphous silica (Figure S4). Interestingly, all MOPs@SBA-16 composites present the same patterns as pristine SBA-16, which is quite different from bulk MOPs. The absence of diffraction peaks in MOPs@SBA-16 composites reveals that MOPs are highly dispersed in SBA-16. On the basis of these results, it is clear that MOPs are successfully introduced and well dispersed in mesoporous silica.

The MOPs@SBA-16 composites exhibit a type-IV isotherm with an H2-type hysteresis loop, which is similar to pristine SBA-16 (Figure 3a). Due to the aggregation of bulk MOP molecules, MOP-SO$_3$H presents negligible N$_2$ uptake. In comparison with pristine SBA-16, the hysteresis loop shifts to lower relative pressure after the introduction of MOPs. The pore size distributions give more apparent evidence of the location of MOP molecules (Figure 3b). Pristine SBA-16 shows two pore size distributions at 2.0 and 6.5 nm, which are caused by pore entrances and cavities, respectively. It is interesting to note that the introduction of MOPs leads to the decrease of cavity size from 6.5 to 5.8 nm (MS-SO$_3$H) and 5.3 nm (M′S-SO$_3$H), while
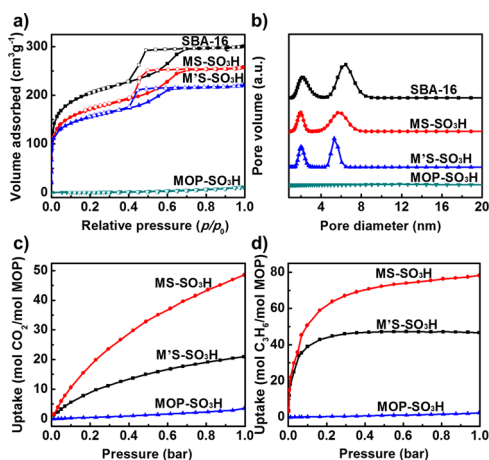
Figure 3. (a) N_2 adsorption−desorption isotherms at 77 K; (b) pore size distributions; (c) CO_2 adsorption isotherms at 273 K; and (d) C_3H_6 adsorption isotherms at 273 K. The C_3H_6 and CO_2 adsorption capacities of MS-SO$_3$H and M′S-SO$_3$H (mol adsorbate/mol MOP) were calculated by subtracting the uptake of support from the measured uptake.

the size of pore entrances keeps unchanged (Table S1). These results thus clearly show that MOPs are successfully introduced to cavities rather than entrances of mesoporous silica, which is of great importance for the formation of isolated MOP molecules in confined spaces. It is worth noting that the reduction of cavity size is relatively small and the silica cavities are not proportional to the size and number of MOPs introduced. This is because MOPs themselves are porous and N_2 molecules can also enter the pores of MOPs during measurement. As a result, the pores of MOPs also contribute to the overall pore size distributions of composites. This can also explain that different MOPs do not reduce the cavity size of SBA-16 proportional to the MOP size.

To probe the dispersion state of MOPs in confined spaces, the adsorption of two gas molecules (i.e., CO_2 and C_3H_6) was carried out (Figure 3c,d). CO_2 is considered an anthropogenic greenhouse gases,[10] while C_3H_6 is one of the most important industrial chemicals;[11] both of them need to be adsorbed selectively from corresponding mixtures. For bulk MOPs, a negligible amount of CO_2 is adsorbed, because of the aggregation of MOP molecules and the blockage of active sites. It is worth noting that MOPs confined in silica cavities exhibit much better CO_2 adsorption capacity. To avoid the influence of support on the comparison, CO_2 and C_3H_6 adsorption capacities of the composites were calculated by subtracting the uptake of supoport from the measured uptake. In the composite MS-SO$_3$H, the uptake reaches 48 mol CO_2/mol MOP. Taking into account that one MOP-SO$_3$H molecule consists of 24 copper sites and 24 sulfonic groups, one copper site/sulfonic group can capture one CO_2 molecule. This means that MOP molecules are highly dispersed and form isolated state in silica cavities, so that all of the active sites are well-exposed. Because the CO_2 uptake in the present study is per mole of MOP, the uptakes correlate well with the dispersion degree of MOPs. In the case of the composite M′S-SO$_3$H, there is more than one MOP molecule in each cavity, and the dispersion degree of MOP is thus declined. Accordingly, the CO_2 uptake for MOPs in the composite M′S-SO$_3$H is less than that in MS-SO$_3$H. Similar results were also observed in the adsorption of C_3H_6. Interestingly, the C_3H_6 uptake of MOPs in the composite MS-SO$_3$H is 78 mol C_3H_6/mol MOP. This means in addition to metal and ligand sites, the pores of MOPs are also

able to capture C_3H_6. These results demonstrate that active sites are highly accessible for well-dispersed MOPs in confined cavities.

The resultant materials were applied to catalyze the synthesis of 2-methoxy-2-phenylethanol (MPE) from the ring opening of styrene oxide. MPE is a valuable intermediate widely used in pharmaceutical and chemical industries.[12] Because of the coordinatively unsaturated metal active sites, MOPs may be a good candidate for catalyzing ring-opening reactions. No styrene oxide was converted at all on SBA-16, owing to the absence of active sites (Figure 4a). In the case of MOP-SO$_3$H, the
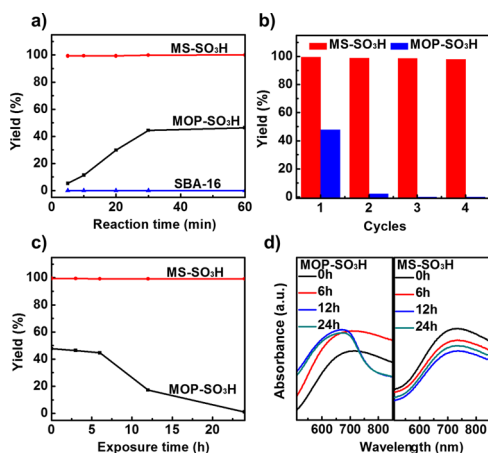
Figure 4. (a) Catalytic performance of SBA-16, MOP-SO$_3$H, and MS-SO$_3$H on the ring opening of styrene oxide. (b) Reusability of MOP-SO$_3$H and MS-SO$_3$H. (c) Catalytic performance and (d) UV−vis spectra of MOP-SO$_3$H and MS-SO$_3$H after exposure to humid atmosphere (relative humidity = 50%) for 24 h.

conversion of styrene oxide is 48% at 60 min, indicating the existence of catalytic active sites. It is noticeable that under the catalysis of the composite MS-SO$_3$H, the conversion of styrene oxide reaches 100%, which is obviously higher than that over MOP-SO$_3$H and SBA-16. In addition to the difference in conversion of styrene oxide, the reaction rate is also quite different for MOPs before and after introduced to SBA-16. By using MOP-SO$_3$H as the catalyst, the conversion of styrene oxide is 11% at 10 min, which accounts for 23% of the conversion at 60 min. Nevertheless, the composite MS-SO$_3$H can convert 100% of styrene oxide even at 10 min, which is equal to the conversion at 60 min. In other words, when the composite MS-SO$_3$H is employed as catalyst, all reactions take place at the initial stage (within 10 min). Nonetheless, the conversion of styrene oxide over MOP-SO$_3$H increases gradually with reaction time. On the basis of these results, it is conclusive that the catalytic performance of the composite MOPs@SBA-16 is apparently better than bulk MOPs with regard to both reaction conversion and rate.

Because reusability is an important factor influencing the practical applications of heterogeneous catalysts, the catalytic activity of recovered MOPs and MOPs@SBA-16 composites was evaluated. The conversion of styrene oxide remains constant in the four consecutive cycles over the composite MS-SO$_3$H (Figure 4b). The Cu content in the filtrate of reaction mixture was below the detection limits of ICP. This indicates no leaching of Cu from the solid catalysts. In the case of MOP-SO$_3$H, however, the conversion of styrene oxide was sharply reduced (from 48% to 2%) only after one cycle. These results

demonstrate the excellent reusability of MOPs@SBA-16 composites in the ring-opening reaction. The exposure to humid atmosphere results in the damge of MOP-SO₃H structure, while the structure of MS-SO₃H composite is well preserved, as discussed later. As a result, the excellent reusability of MOPs@SBA-16 composites should be ascribed to their high stability.

It is known that Cu-based MOPs are stable in the synthetic solvents, but the structure tends to collapse when exposed to humid atmosphere, which limits the applications of MOPs severely. To examine the stability, both MOPs and MOPs@SBA-16 composites were exposed to humid atmosphere for 24 h. After exposure, both catalytic activity and structure were used to evaluate the stability. For MOP-SO₃H after exposure in humid atmosphere, the conversion of styrene oxide decreased sharply from 48% to 17% (12 h) and 1% (24 h, Figure 4c). Under the same conditions, nonetheless, the catalytic activity of the composite MS-SO₃H remained unchanged. UV–vis technique was also employed to characterize the samples after exposure to humid atmosphere. When MOP-SO₃H was exposed for 12 h, the adsorption peak at 695 nm ascribed to the dicopper paddlewheel shifted to 665 nm, suggesting the damage of structure (Figure 4d). For the composite MS-SO₃H, however, there is no change in the position of adsorption peak at 695 nm even after exposure for 24 h. Further increasing the exposure time to 7 days, the structure of silica-confined MOPs is also well preserved (Figure S5). This confirms the reaction results and indicates that the stability of MOP is greatly improved after confinement in silica cavities.

In addition to MOP-SO₃H, three other MOPs with an identical geometry but different ligand functionality (namely hydroxyl, *tert*-butyl, and amino groups) were also introduced to the cavities of SBA-16 (details in Supporting Informaiton). The DS strategy should enable various supramolecular architectures to be confined in the cavities of porous supports by judicious choice of pore structure parameters. This may lead to the fabrication of isolated architectures with unusual dispersity and stability that are desirable for adsorptive and catalytic applications but unlikely to realize for their bulk counterparts.

■ ASSOCIATED CONTENT

Ⓢ Supporting Information

The Supporting Information is available free of charge on the ACS Publications website at DOI: 10.1021/jacs.6b01207.

Experimental details and data (PDF)

■ AUTHOR INFORMATION

Corresponding Authors

*lbsun@njtech.edu.cn
*jrli@bjut.edu.cn

Notes

The authors declare no competing financial interest.

■ ACKNOWLEDGMENTS

■ REFERENCES

(1) (a) Cook, T. R.; Zheng, Y.-R.; Stang, P. J. *Chem. Rev.* **2013**, *113*, 734. (b) Chakrabarty, R.; Mukherjee, P. S.; Stang, P. J. *Chem. Rev.* **2011**, *111*, 6810. (c) Fujita, M. *Chem. Soc. Rev.* **1998**, *27*, 417. (d) Yoshizawa, M.; Klosterman, J. K.; Fujita, M. *Angew. Chem., Int. Ed.* **2009**, *48*, 3418. (e) Ramsay, W. J.; Szczypiński, F. T.; Weissman, H.; Ronson, T. K.; Smulders, M. M. J.; Rybtchinski, B.; Nitschke, J. R. *Angew. Chem., Int. Ed.* **2015**, *54*, 5636. (f) Ahmad, N.; Chughtai, A. H.; Younus, H. A.; Verpoort, F. *Coord. Chem. Rev.* **2014**, *280*, 1. (g) Kang, S.; Zheng, H.; Liu, T.; Hamachi, K.; Kanegawa, S.; Sugimoto, K.; Shiota, Y.; Hayami, S.; Mito, M.; Nakamura, T.; Nakano, M.; Baker, M. L.; Nojiri, H.; Yoshizawa, K.; Duan, C.; Sato, O. *Nat. Commun.* **2015**, *6*, 5955. (h) Pasquale, S.; Sattin, S.; Escudero-Adan, E. C.; Martinez-Belmonte, M.; de Mendoza, J. *Nat. Commun.* **2012**, *3*, 785. (i) Cook, T. R.; Stang, P. J. *Chem. Rev.* **2015**, *115*, 7001.

(2) (a) Ahmad, N.; Younus, H. A.; Chughtai, A. H.; Verpoort, F. *Chem. Soc. Rev.* **2015**, *44*, 9. (b) Qiu, X.; Zhong, W.; Bai, C.; Li, Y. *J. Am. Chem. Soc.* **2016**, *138*, 1138. (c) Kohyama, Y.; Murase, T.; Fujita, M. *J. Am. Chem. Soc.* **2014**, *136*, 2966. (d) Roukala, J.; Zhu, J.; Giri, C.; Rissanen, K.; Lantto, P.; Telkki, V.-V. *J. Am. Chem. Soc.* **2015**, *137*, 2464. (e) Vardhan, H.; Yusubov, M.; Verpoort, F. *Coord. Chem. Rev.* **2016**, *306*, 171. (f) Takao, K.; Suzuki, K.; Ichijo, T.; Sato, S.; Asakura, H.; Teramura, K.; Kato, K.; Ohba, T.; Morita, T.; Fujita, M. *Angew. Chem., Int. Ed.* **2012**, *51*, 5893. (g) Sun, L.-B.; Li, J.-R.; Lu, W.; Gu, Z.-Y.; Luo, Z.; Zhou, H.-C. *J. Am. Chem. Soc.* **2012**, *134*, 15923.

(3) (a) Aijaz, A.; Karkamkar, A.; Choi, Y. J.; Tsumori, N.; Ronnebro, E.; Autrey, T.; Shioyama, H.; Xu, Q. *J. Am. Chem. Soc.* **2012**, *134*, 13926. (b) Park, J.; Sun, L.-B.; Chen, Y.-P.; Perry, Z.; Zhou, H.-C. *Angew. Chem., Int. Ed.* **2014**, *53*, 5842. (c) Shekhah, O.; Belmabkhout, Y.; Chen, Z.; Guillerm, V.; Cairns, A.; Adil, K.; Eddaoudi, M. *Nat. Commun.* **2014**, *5*, 4228.

(4) (a) Zhao, D.; Tan, S.; Yuan, D.; Lu, W.; Rezenom, Y. H.; Jiang, H.; Wang, L. Q.; Zhou, H. C. *Adv. Mater.* **2011**, *23*, 90. (b) Liu, T. F.; Chen, Y. P.; Yakovenko, A. A.; Zhou, H. C. *J. Am. Chem. Soc.* **2012**, *134*, 17358.

(5) (a) Sun, L. B.; Liu, X. Q.; Zhou, H. C. *Chem. Soc. Rev.* **2015**, *44*, 5092. (b) Mohanty, P.; Li, D.; Liu, T.; Fei, Y.; Landskron, K. *J. Am. Chem. Soc.* **2009**, *131*, 2764. (c) Deng, Y.; Wei, J.; Sun, Z.; Zhao, D. *Chem. Soc. Rev.* **2013**, *42*, 4054. (d) Kim, J.; Kim, B.; Anand, C.; Mano, A.; Zaidi, J. S. M.; Ariga, K.; You, J.; Vinu, A.; Kim, E. *Angew. Chem.* **2015**, *127*, 8527.

(6) (a) Zhang, M.; Gu, Z.-Y.; Bosch, M.; Perry, Z.; Zhou, H.-C. *Coord. Chem. Rev.* **2015**, *293–294*, 327. (b) Shakeri, M.; Klein Gebbink, R. J.; de Jongh, P. E.; de Jong, K. P. *Angew. Chem.* **2013**, *125*, 11054. (c) Yang, H.; Zhang, L.; Zhong, L.; Yang, Q.; Li, C. *Angew. Chem., Int. Ed.* **2007**, *46*, 6861. (d) Wu, C. M.; Rathi, M.; Ahrenkiel, S. P.; Koodali, R. T.; Wang, Z. *Chem. Commun.* **2013**, *49*, 1223.

(7) (a) Kleitz, F.; Czuryszkiewicz, T.; Solovyov, L. A.; Lindén, M. *Chem. Mater.* **2006**, *18*, 5070. (b) Kleitz, F.; Kim, T.-W.; Ryoo, R. *Langmuir* **2006**, *22*, 440. (c) Sakamoto, Y.; Kaneda, M.; Terasaki, O.; Zhao, D. Y.; Kim, J. M.; Stucky, G.; Shin, H. J.; Ryoo, R. *Nature* **2000**, *408*, 449. (d) Zhao, D.; Huo, Q.; Feng, J.; Chmelka, B. F.; Stucky, G. D. *J. Am. Chem. Soc.* **1998**, *120*, 6024.

(8) Li, J. R.; Zhou, H. C. *Nat. Chem.* **2010**, *2*, 893.

(9) Sobczak, I.; Wolski, Ł. *Catal. Today* **2015**, *254*, 72.

(10) (a) Hwang, C.-C.; Tour, J. J.; Kittrell, C.; Espinal, L.; Alemany, L. B.; Tour, J. M. *Nat. Commun.* **2014**, *5*, 3961. (b) McDonald, T. M.; Mason, J. A.; Kong, X.; Bloch, E. D.; Gygi, D.; Dani, A.; Crocella, V.; Giordanino, F.; Odoh, S. O.; Drisdell, W. S.; Vlaisavljevich, B.; Dzubak, A. L.; Poloni, R.; Schnell, S. K.; Planas, N.; Lee, K.; Pascal, T.; Wan, L. F.; Prendergast, D.; Neaton, J. B.; Smit, B.; Kortright, J. B.; Gagliardi, L.; Bordiga, S.; Reimer, J. A.; Long, J. R. *Nature* **2015**, *519*, 303. (c) Haszeldine, R. S. *Science* **2009**, *325*, 1647.

(11) (a) Jiang, W.-J.; Yin, Y.; Liu, X.-Q.; Yin, X.-Q.; Shi, Y.-Q.; Sun, L.-B. *J. Am. Chem. Soc.* **2013**, *135*, 8137. (b) Chang, G.; Huang, M.; Su, Y.; Xing, H.; Su, B.; Zhang, Z.; Yang, Q.; Yang, Y.; Ren, Q.; Bao, Z.; Chen, B. *Chem. Commun.* **2015**, *51*, 2859.

(12) (a) Tokunaga, M.; Larrow, J. F.; Kakiuchi, F.; Jacobsen, E. N. *Science* **1997**, *277*, 936. (b) Zu, D.-D.; Lu, L.; Liu, X.-Q.; Zhang, D.-Y.; Sun, L.-B. *J. Phys. Chem. C* **2014**, *118*, 19910.